Published in final edited form as:

Cancer Res. 2016 June 1; 76(11): 3211–3223. doi:10.1158/0008-5472.CAN-15-0025.

Radiation sensitivity in a preclinical mouse model of medulloblastoma relies on the function of the intrinsic apoptotic pathway

Andrew Crowther, BS[1,*], **Jennifer Ocasio, BS**[1,2,*], **Fang Fang, PhD**[3], **Jessica Meidinger, BS**[2], **Jaclyn Wu**[2], **Allison M Deal, MS**[4], **Sha X. Chang, PhD**[4,5], **Hong Yuan, PhD**[4,6], **Ralf Schmid, PhD**[7], **Ian Davis, MD, PhD**[4,8], and **Timothy R. Gershon, MD, PhD**[1,2,4]

[1]UNC Neuroscience Center, University of North Carolina School of Medicine, Chapel Hill, North Carolina, USA 27599

[2]Department of Neurology, University of North Carolina School of Medicine, Chapel Hill, North Carolina, USA 27599

[3]Department of Genetics, University of North Carolina School of Medicine, Chapel Hill, North Carolina, USA 27599

[4]Lineberger Comprehensive Cancer Center, University of North Carolina School of Medicine, Chapel Hill, North Carolina, USA 27599

[5]Department of Radiation Oncology, University of North Carolina School of Medicine, Chapel Hill, North Carolina, USA 27599

[6]Department of Radiology, University of North Carolina School of Medicine, Chapel Hill, North Carolina, USA 27599

[7]Department of Pathology, University of North Carolina School of Medicine, Chapel Hill, North Carolina, USA 27599

[8]Department of Pediatrics, University of North Carolina School of Medicine, Chapel Hill, North Carolina, USA 27599

Abstract

While treatments that induce DNA damage are commonly used as anti-cancer therapies, the mechanisms through which DNA damage produces a therapeutic response are incompletely understood. Here we have tested whether medulloblastomas must be competent for apoptosis to be sensitive to radiation therapy. Whether apoptosis is required for radiation sensitivity has been controversial. Medulloblastoma, the most common malignant brain tumor in children, is a biologically heterogeneous set of tumors typically sensitive to radiation and chemotherapy; 80% of medulloblastoma patients survive long-term after treatment. We used functional genetic studies to determine if the intrinsic apoptotic pathway is required for radiation to produce a therapeutic

Corresponding Author: Timothy R. Gershon, MD, PhD, Dept. of Neurology, CB 7025, UNC School of Medicine, Chapel Hill, NC 27599, ; Email: gershont@neurology.unc.edu, PHONE: (919) 966-3618, FAX: (919) 966-2922

*authors contributed equally to the work

The authors report no conflicts of interest.

response in mice with primary, Shh-driven medulloblastoma. We found that cranial radiation extended the survival of medulloblastoma-bearing mice and induced widespread apoptosis. Expression analysis and conditional deletion studies showed that p53 was the predominant transcriptional regulator activated by radiation and was strictly required for treatment response. Deletion of Bax, which blocked apoptosis downstream of p53, was sufficient to render tumors radiation resistant. In apoptosis-incompetent, Bax-deleted tumors, radiation activated p53-dependent transcription without provoking cell death and caused two discrete populations to emerge. Most radiated tumor cells underwent terminal differentiation. Perivascular cells, however, quickly resumed proliferation despite p53 activation, behaved as stem cells, and rapidly drove recurrence. These data show that radiation must induce apoptosis in tumor stem cells to be effective. Mutations that disable the intrinsic apoptotic pathways are sufficient to impart radiation resistance. We suggest that medulloblastomas are typically sensitive to DNA-damaging therapies because they retain apoptosis competence.

Introduction

Whether DNA-damaging anti-cancer treatments must induce apoptosis to be clinically beneficial remains an unsettled question with important implications. Because resistance to apoptosis is recognized as a hallmark of cancer [1, 2], it has been proposed that radiation and chemotherapy act through non-apoptotic mechanisms, including mitotic catastrophe, senescence, and necrosis [3, 4]. If tumor cells die through non-apoptotic mechanisms the active participation of the tumor cell may not be required; for example injury may accumulate until cell viability is compromised. Apoptosis, in contrast, requires the function of endogenous molecular pathways within the tumor cell. If apoptosis is required for treatment response, resistance to therapy may arise from any mutation that disrupts the apoptotic pathways.

Medulloblastoma, the most common malignant brain tumor in children, is an ideal cancer in which to examine the role of apoptosis in treatment response, because most medulloblastomas are strikingly sensitive to DNA-damaging therapies. Whereas medulloblastoma was invariably fatal before the use of external beam radiation (xRT) , radiation of the entire neuraxis results in 60% long-term survival [5]. The addition of chemotherapy to xRT further increases the 5-year event-free survival (EFS) to 81% [6]. In contrast, for children with glioblastoma, xRT and chemotherapy produce a 3-year EFS of 7% [7]. The biologic basis for the specific sensitivity of medulloblastoma to conventional therapy is unknown, and in every molecular subgroup of medulloblastoma, outcomes are heterogeneous [8]. Determining the cellular processes required for medulloblastoma to respond to xRT may lead to alternative, less toxic therapeutic approaches and to new ways to identify and address the 20% of patients with resistant tumors.

Insight into the molecular pathogenesis of medulloblastoma has made it possible to generate transgenic mice that develop primary medulloblastoma with high incidence and short latency [9–13]. Aberrant activation of the Sonic Hedgehog (SHH) signaling pathway defines a molecular subgroup that includes patients with sporadic and familial tumors, overall 28% of patients [14]. Constitutive activation of the Shh pathway in neural progenitors in transgenic

mice causes tumors that faithfully recapitulate the SHH-subgroup of human medulloblastoma, sharing a common site of origin, histology and molecular signature. Transgenic, conditional SmoM2 mice, express a mutant, constitutively active allele of the Shh receptor component Smoothened, when activated by cre recombinase [15]. Mice with the genotype Math1-cre;SmoM2 (M-Smo) express SmoM2 in cerebellar granule neuron progenitors and develop medulloblastoma with 100% frequency by postnatal day 12 (P12) [16], providing a highly efficient preclinical model. Deleting specific genes in M-Smo mice offers a genetic approach to identify molecular determinants of tumor response.

Prior studies in primary tumor models of both medulloblastoma and lymphoma have shown that p53 function is essential for treatment effectiveness [17–20]. Many cancers with intact p53, however, are treatment resistant. Diverse cellular processes may be engaged by p53 activation after treatment, including both apoptosis and cell cycle exit [21]. Testing the functional role of specific mechanisms that operate downstream of p53 in mediating treatment sensitivity may identify new mechanisms of resistance to therapy. Here, we directly tested the importance of the intrinsic apoptosis pathway in a primary tumor model *in vivo*. We subjected mice with Shh-driven medulloblastomas to xRT, determined that this treatment elicited a p53-dependent response, and then examined the effect of deleting the apoptosis gatekeeper protein Bax. While Bax mutations have not been identified in medulloblastoma, Bax deletion served in our model as a genetically tractable method of blocking apoptosis; numerous genetic and epigenetic events may effectively block apoptosis in the human disease. We used this genetic approach to determine if a functional intrinsic apoptotic pathway is required for xRT to produce a clinically significant benefit.

We modeled radiation therapy by subjecting M-Smo mice with primary medulloblastoma to cranial xRT. We found that 10Gy of radiation, delivered in either 1 dose or in 5 fractions of 2 Gy, produced a strong anti-tumor effect. Transcriptomic analysis prior to the onset of apoptosis demonstrated that xRT induced a pattern of gene expression changes that was highly dependent on p53 regulation and included both pro-apoptotic and anti-proliferative components. Conditional deletion of either p53 or Bax blocked the therapeutic benefit of xRT, demonstrating the importance of p53-induced activation of endogenous apoptotic pathways in mediating medulloblastoma treatment sensitivity.

Methods

Mice

All animals were handled and used in accordance with approved practices of the Animal Care and Use Committee of the University of North Carolina (IACUC# 13–121). Math1-cre mice [46] were shared by David Rowitch (UCSF, San Francisco, CA) and Robert Wechsler-Reya (Sanford-Burnham Medical Research Institute, La Jolla, CA). Bax floxed ($Bax^{fl/fl}$) mice (strain:6329), SmoM2 mice (strain:5130), and p53 floxed ($p53^{fl/fl}$) mice (strain:8462) were purchased from Jackson Laboratories, Bar Harbor, ME, USA. All mice were maintained on a C57/Bl6 background through at least 4 crosses and both sexes were used for experiments. Genotypes were determined by PCR using Tail Lysis Buffer (Allele Biotechnology, cat#ABP-PP-MT01) and genotyping protocols from Jackson Labs (jaxmice.jax.org).

xRT treatment

Tumor-bearing pups at P12 were administered continuous anesthesia (Isoflurane, 1.5%) for 4 min. inside a small animal research irradiator (RS 2000, Rad Source Technologies) that delivered an x-ray dose of either 2 Gy or 10Gy, centered on the posterior fossa, with the dose rate of 2.6 Gy/min. Cranial radiation was achieved by shielding the body of the animal with a lead plate. 2Gy doses were repeated daily to a total dose of 10 Gy. Sham-treated mice were administered anesthesia without xRT. Mice were heated and monitored while recovering from anesthesia and returned to their home cage for survival studies.

Kaplan Meier survival analysis

Tumor-bearing mice were monitored daily for health status and movement abnormalities. All mice were euthanized at the onset of symptoms, including 10% weight loss, ataxia or lethargy. The age of the animal at the time of harvest due to tumor symptoms was recorded as the event-free survival. The Kaplan-Meier method was used to estimate survival and Log Rank tests were used to compare survival between experimental groups.

Histology

Tissue was collected for histology at indicated times after xRT and processed for immunohistochemistry (IHC) as previously described [24]. Briefly, brains were fixed in 4% formaldehyde in PBS for 24 hours then embedded in paraffin and sectioned. IHC was performed on paraffin-embedded sections after deparaffinization in Histoclear and rehydration in a graded ethanol series, heated to boiling in 10 mM citrate buffer, pH 6.0, in a pressure cooker for 15 min. After antigen retrieval, IHC was performed using primary antibodies: phosphorylated histone H2AX (γH2AX) (cat#9718, Cell Signaling Technology, Danvers, MA, USA), Bax (cat#AF820, Sigma, St. Louis, MO, USA), p53 (cat#2527, Cell Signaling Technology), cleaved Caspase 3 (cC3) (cat#9664, Cell Signaling Technology), NeuN (cat#MAB377, EMD Millipore, Billerica, MA, USA), p21 (cat#ab109199, Abcam, Cambridge, UK), Proliferating Cell Nuclear Antigen (PCNA; cat#2586, Cell Signaling Technology), phosphorylated Histone H3 (pH3; cat#9701, Cell Signaling Technology), phosphorylated p53 (p-p53 ; cat #9284, Cell Signaling Technology), and Sox2 (cat # AB5603, EMD Millipore). H&E-stained sections were prepared using standard techniques. TUNEL staining was performed per manufacturer's protocol (cat#C10245, Life technologies, Carlsbad CA). Where indicated, nuclei were counterstained with 4′6-diamino-2-phenylindole (DAPI; cat#D1306, Life technologies), diluted 200 ng/ml in PBS for 5 min. Stained slides were scanned using an Aperio ScanScope XT and imaged using Aperio ImageScope software (Aperio, Vista, CA, USA).

Expression arrays and analysis

Tumor tissue was dissected and immediately flash frozen at indicated times after xRT. Frozen tissue was homogenized by sonication in RLT buffer (Qiagen), and total RNA was purified following manufacturer's instructions (QIAGEN, cat#74104). RNA was labeled, hybridized to Affymetrix Mouse Gene 2.1^{ST} arrays, per manufacturer's protocol (Affymetrix, Santa Clara, CA USA) and scanned by the UNC-Lineberger Genomics core.

Microarray analysis was performed using R (http://www.r-project.org/) and Bioconductor (http://www.bioconductor.org/) for independent SmoM2 mice without radiation (n = 6) and SmoM2 mice 2 hours after radiation (n = 6). T-test was used to identify genes that change significantly between the two groups. A list of 123 genes identified in this analysis with increased RNA abundance after radiation was used to identify potentially enriched biologic processes using the GSEA software [47]. The Affymetrix gene expression dataset has been deposited in GEO.

For RT-qPCR, cDNA was prepared from total RNA using oligo-dT primers and the Superscript III kit (Life Technologies, Cat# 18080400) per manufacturer's instructions. SYBR-green qPCR was then run on cDNA, using primer sequences: p21-CAGCAGAATAAAAGGTGCCACA, GACAACGGCACACTTTGCTC; PUMA-AGGTGCCTCAATAGCAACCC, CTCCCTGGAGCCCCG, β2 Microglobulin-CTCGGTGACCCTGGTCTTTC,TTGAGGGGTTTTCTGGATAGCA, GAPDH-AAGAGGGATGCTGCCCTTAC, CGGGACGAGGAAACACTCTC.

In situ hybridization

PUMA and p21 mRNA were detected by *in situ* hybridization using the RNAScope 2.0 HD Brown Assay kit (Cat# 300056, Advanced Cell Diagnostics, Hayward CA, USA). Probes for PUMA (Cat# 300031) and p21(Cat# 408551) were obtained from Advanced Cell Diagnostics and used per manufacturer's protocol, including RNAse-free DNAse treatment.

In-vivo treatments

Etoposide—Tumor-bearing pups at P12 were dosed with 5mg/kg etoposide (cat#E1383, Sigma) in saline solution containing 1% DMSO. A single 50ul intraperitoneal injection of etoposide was given; 8 hours after injection tissue was harvested for histology.

BrdU/EdU labeling—A single 400mg/kg dose of BrdU (cat#B5002, Sigma) and, 2 days later, a single dose of 400mg/kg EdU (cat#A10044, Life technologies), both in 100ul of saline solution, were given by intraperitoneal injection at time points indicated in text. Double labeling was accomplished through standard histological processing using a monoclonal primary antibody against BrdU (cat#5292, Cell Signaling Technology) and Click-iT® chemistry for labeling of EdU (cat#C10337, Life technologies).

Results

Mouse medulloblastoma, like human medulloblastoma, responds to xRT with increased survival time

We have previously shown that a single fraction of 10 Gy induces a wave of apoptosis in M-Smo medulloblastomas after a latent period of 3–4 hours [22]. To determine if radiation produced a sustained regression, consistent with a clinically relevant benefit, we compared survival of M-Smo mice with or without xRT. At P12, tumor-bearing mice were randomly assigned to receive xRT (n=34) or no treatment (n=23). We subjected mice in the xRT group to 10 Gy cranial irradiation, focused on the posterior fossa. Control mice were subjected to sham treatment with anesthesia without irradiation. xRT increased median survival from 20

to 36 days ($p<0.001$; Log rank test) with 15% of treated mice surviving disease free for > 100 days (Figure 1A). A separate set of mice treated with 10 Gy administered as 5 daily fractions of 2Gy showed a similar increase in survival ($p<0.001$; Log rank test; Figure 1A'.)

Histologic analysis demonstrated a temporal pattern of radiation response that was consistent from animal to animal. We examined 3 biologic replicates at progressive intervals after single-fraction treatment. We found that tumors became less densely cellular by 4 hours after treatment with 10Gy xRT, decreased in size by 24 hours, and involuted by 5 days (Figure 1B–E). Prior to xRT, rare, scattered tumor cells demonstrated spontaneous DNA damage as determined by IHC for γH2AX; after xRT, all tumor cells and adjacent neurons stained strongly for γH2AX in 3/3 mice, indicating widespread DNA damage (Figure 1F,G). The increased γH2AX signal dissipated by 24 hours after xRT in 3/3 mice as tumor cells underwent cell death and neurons completed the repair of DNA damage (Figure 1H,I). Tumor cell apoptosis, demonstrated by IHC for cC3, began at 4 hours after xRT in all mice examined, and persisted over the first 24 hours after treatment (Figure 1J–M). TUNEL staining also demonstrated cell death beginning 4 hours after xRT (Supplementary Fig. S1A). Treatment with a single fraction of 2Gy produced similar, but more heterogeneous patterns of TUNEL staining, DNA damage and cell death 4 hours after xRT (Supplementary Fig. S1B–F). Thus, 2Gy and 10Gy doses of xRT provoked tumor cell apoptosis in mouse medulloblastoma after a latent period of less than 4 hours, and a cumulative dose of 10Gy significantly extended mouse survival.

The transcriptional response of medulloblastomas to xRT is predominantly driven by p53 and includes regulators of apoptosis and cell cycle progression

To define the early molecular events mediating the tumor response to xRT, we compared mRNA isolated from medulloblastomas 2 hours after xRT or from untreated control tumors. 10 Gy cranial xRT was administered to tumor-bearing M-Smo mice (n = 6). RNA was isolated from tumors 2 hours after treatment, prior to the onset of apoptosis, defined by detectable cleavage of caspase 3. For comparison, RNA was isolated from an equal number of littermate, sham-treated controls. RNA was analyzed on Affymetrix Mouse Gene 2.1ST expression arrays. The mRNA levels of 123 genes were increased by 1.5 fold or greater after xRT, with a corrected p-value < 0.01 (Figure 2A). GSEA analysis demonstrated a significant concordance between these genes and previously published p53-related gene sets (Figure 2B and Supplementary Table 1–3). Previously identified p53 targets demonstrated significantly greater fold change after xRT compared to the entire set of genes analyzed (Figure 2C). This association was observed for a set of 52 genes that were identified from published literature as p53-induced (Supplementary Table 1), and for a set of 163 genes detected in a recent GRO-seq analysis of p53 targets (Supplementary Table 2) [23]. As a control, a gene set randomly drawn from 10 unrelated MSigDB sets (control gene set, Supplementary Table 4) demonstrated no difference in RNA fold change. Ingenuity Pathway Analysis similarly identified p53 as the upstream regulator most strongly activated by xRT, with 26/73 consensus p53 targets up-regulated ($p = 1.3x10^{-19}$); no other upstream regulators were identified with the significance within 3 orders of magnitude. Together, these pathway- and gene-specific comparisons demonstrated that xRT-induced RNA changes were highly associated with p53 response.

Among the p53 target genes that were strongly up-regulated in response to xRT were the pro-apoptotic genes (Apaf: FC=1.9, $p=4.2x10^{-6}$; Bax: FC=1.9, $p=9.7x10^{-7}$; PUMA: FC=3.8, $p=2.8x10^{-7}$), and inhibitors of cell cycle progression (p21/Cdkn1A: FC=3.9, $p=1.2x10^{-8}$). Using quantitative PCR we confirmed that PUMA and p21 mRNA were increased 8 and 6 fold, respectively, after xRT (Figure 2D). These data show that xRT activated a coherent, reproducible transcriptional profile in medulloblastoma that was driven largely by p53 and included genes promoting both cell death and cell cycle arrest.

To confirm the essential role of p53 in the response to xRT in our model, we bred mice with conditional alleles of p53 into Math1-cre and SmoM2 lines to generate homozygous, Math1-cre;SmoM2;$p53^{f/f}$ (M-Smo;$p53^{floxed}$) mice and heterozygous Math1-cre;SmoM2;$p53^{f/+}$ littermate controls (M-Smo;$p53^{het}$) . Both genotypes developed tumors with 100% frequency by P12. We treated both genotypes with 10 Gy xRT and examined 3 biologic replicates of each genotype at specific intervals after treatment. Radiation induced homogeneous accumulation of p53 protein in all M-Smo;$p53^{het}$ tumors within 2 hours (Figure 3A,B). As expected, in M-Smo;$p53^{floxed}$ tumors, p53 protein was absent from tumor cells and only accumulated in endothelial cells of tumor capillaries (Figure 3C,D). Induction of both PUMA and p21 after xRT was significantly reduced in 3/3 M-Smo;$p53^{floxed}$ tumors (Figure 3E–J). In 3/3 p53-deleted tumors at 4 hours, 24 hours or 5 days after xRT, radiation did not provoke widespread apoptosis, although some cell death in stroma was observed at 4 hours (Figure 3K–M). In contrast, 3/3 M-Smo;$p53^{het}$ tumors responded to xRT with precipitous apoptosis, similar to tumors with wild type p53 (data not shown). Proliferation was transiently suppressed by xRT in M-Smo;$p53^{floxed}$ tumors, as mitoses were undetectable in all tumor 4 hours after radiation (Figure 3N). Mitosis resumed by 24 hours, however, and continued at 5 days (Figure 3O,P). Although xRT induced transient cell cycle arrest in M-Smo;$p53^{floxed}$ tumors, this growth arrest was not sustained. These results show that p53 was required for xRT to produce a durable therapeutic response.

The therapeutic effect of xRT requires a functional intrinsic apoptotic pathway

To determine if the intrinsic apoptotic pathway was required for the p53-mediated response of medulloblastoma to radiation, we next examined the effect of xRT on tumor-bearing mice with conditional deletion of the pro-apoptotic protein Bax. Mice with floxed alleles of Bax were bred into a Math1-cre and SmoM2 background to generate homozygous, Math1-cre;SmoM2;$Bax^{f/f}$ (M-Smo;Bax^{floxed}) mice and homozygous Math1-cre;SmoM2;$Bax^{+/+}$ littermate controls (M-Smo;Bax^{WT}). Bax protein was absent in M-Smo;Bax^{floxed} tumors, and Bax deletion did not alter tumor histology (Supplementary Figure S2A–D). IHC for cC3, however, demonstrated that spontaneous apoptosis was markedly reduced (Supplementary Figure S2E,F). We did not detect a statistically significant effect of Bax deletion on the survival of mice with Math1-cre;SmoM2-driven tumors (Supplementary Figure S2G). We previously found that Bax deletion accelerated tumorigenesis in the more slowly tumorigenic ND2:SmoA1 mouse line [24]. However, Bax deletion did not accelerate the already rapid tumorigenesis of Math1-cre;SmoM2 mice.

We examined the effect of Bax deletion on survival after xRT by comparing the survival of radiated mice with M-Smo or M-Smo;Bax^{floxed} genotypes. Event-free survival was

significantly shorter in xRT-treated M-Smo;Bax^{floxed} mice and resembled the survival of M-Smo mice without treatment (Figure 4A). Consistent with a lack of clinical benefit, we found no significant difference in the event-free survival of treated and untreated M-Smo;Bax^{floxed} mice (n=10;Log Rank p=0.76). Fractionated xRT, administered as five doses of 2Gy similarly failed to extend the survival of M-Smo;Bax^{floxed} mice, which showed significantly shorter survival compared to M-Smo mice treated with 5 doses of 2Gy (Figure 4A'). These data show that Bax was required for xRT to impart a clinically significant benefit.

To confirm that Bax deletion did not alter the induction of DNA damage or p53 activation, we examined γH2AX and p53. In 3/3 replicate pups of both M-Smo;Bax^{WT} and M-Smo;Bax^{floxed} mice, xRT produced extensive DNA double strand breaks, demonstrated by γH2AX (Figure 4B–D). This DNA damage produced equivalent phosphorylation of p53 (Figure 4E–G). Unlike M-Smo;Bax^{WT} tumors, M-Smo;Bax^{floxed} tumors did not undergo synchronous apoptosis 4 hours after xRT as indicated by relatively little induction of caspase 3 cleavage (Figure 4H–M) or TUNEL staining (Figure 4N–P). In the absence of Bax-dependent apoptosis neither DNA damage *per se*, nor the resulting p53 engagement were sufficient to cause widespread cell death or to extend mouse survival.

To test the possibility that radiation-induced cell death was delayed, rather than prevented in Bax-deleted tumor cells, we examined tumors at greater intervals after treatment, specifically 5 days after single fractions 10Gy or at the end of 5 daily fractions of 2 Gy. Medulloblastomas with intact Bax typically decreased in size within 48 hours after xRT and reached a minimum tumor size by 5 days. In contrast, Bax-deficient tumors consistently persisted as large masses (Figure 5A–C). 48 hours after 10Gy xRT, only scattered cells in M-Smo;Bax^{floxed} tumors demonstrated caspase 3 cleavage (Figure 5D) and scattered cells underwent non-apoptotic cell death, identified by positive TUNEL staining and negative staining for cleavage of caspase 3 (Figure 5D,G). 5 days after xRT, neither cC3 nor TUNEL demonstrated increased cell death (Figure 5 D–I). These results show that latent cell death in Bax-deleted tumors was not widespread and did not significantly disrupt tumor growth.

We further investigated whether the cytotoxic effect of chemotherapy required intact apoptotic pathways. We compared DNA damage and apoptosis in M-Smo;Bax^{floxed} and M-Smo;Bax^{WT} littermates 8 hours after IP etoposide injection (n=3 for each group). Etoposide caused extensive DNA damage in tumors of all treated mice (data not shown). Bax^{WT} tumors demonstrated with extensive apoptosis, whereas in M-Smo;Bax^{floxed} tumors cell death was markedly reduced (Fig 5J,K). Thus, Bax is necessary for apoptosis in response to diverse, DNA-damaging therapies.

Apoptosis-deficient tumor cells resolve after treatment into terminally differentiated and proliferating populations

Examination of replicate M-Smo;Bax^{floxed} tumors at successive intervals after treatment demonstrated the fate of radiated tumor in the absence of apoptosis. Although xRT did not slow the progression of M-Smo;Bax^{floxed} tumors, we noted significant changes in tumor pathology. In 3/3 M-Smo;Bax^{floxed} tumors we found that the xRT-induced phosphorylation of H2AX resolved by 48 hours, indicating that medulloblastoma cells were able to repair

radiation-induced DNA double strand breaks when apoptosis was blocked (Figure 6A,B). By 48 hours after xRT, all 3 Bax-deleted tumors demonstrated histologic changes indicating widespread differentiation. Tumor cells became less densely packed, elaborated eosinophilic neuropil and formed abundant Homer-Wright rosettes (Figure 6C,D). Consistent with terminal differentiation along the expected trajectory of neural progenitors, a large subpopulation within all 3 M-Smo;Bax^{floxed} tumors radiated tumors strongly up-regulated the neuronal marker NeuN (Figure 6E,F).

Despite the widespread differentiation induced by xRT, M-Smo;Bax^{floxed} tumors consistently progressed. Prior studies of RCAS-induced medulloblastomas in mice have shown that these tumors harbor a subpopulation in the perivascular regions that resumes proliferation within 72 hours of treatment with 2Gy xRT [20]. We did not find similar early recurrence after 10Gy in M-Smo mice with intact p53 and Bax. In M-Smo;Bax^{floxed} tumors, however, we found that perivascular cells resumed proliferation after a period of quiescence. In 3/3 M-Smo;Bax^{floxed} mice examined 4 hours after xRT, the p53 target p21 was specifically up-regulated in tumor cells along capillaries (Figure 7A). Expression of p21 persisted through 24 hours, and during this period no cells expressing the proliferation marker PCNA were detected (n = 3). By 48 hours after xRT, 4/6 tumors examined contained PCNA+ cells. In all four tumors, these cells were predominantly located in the perivascular regions (Figure 7B). Double labeling for PCNA and the differentiation marker p27 demonstrated that proliferating and differentiating tumor cells resolved spatially into discrete regions, with proliferation along blood vessels and differentiation further from the perivascular space (Figure 7C). All 9 radiated, M-Smo;Bax^{floxed} mice in the survival study that were harvested at the time of tumor progression demonstrated abundant PCNA+ tumor cells, indicating that after a latent period, proliferation consistently resumed. Taken together, these data show that a proliferative subpopulation, traceable to the perivascular regions, drives tumor recurrence after xRT in our model. These perivascular cells were subject to p53-mediated transcriptional changes, but in the absence of apoptosis, the activation of p53 did not produce lasting therapeutic effects through either non-apoptotic cell death or sustained growth arrest.

To examine the tendency of tumor cells to enter and to exit the cell cycle after xRT, we labeled cells at S phase at 2 discrete time points, using incorporation of BrdU and EdU. M-Smo;Bax^{floxed} mice were injected with BrdU 5 days after xRT, and then injected with EdU 2 days later. Mice were harvested 4 hours after EdU injection. In 3/5 mice, we found that BrdU injection labeled a large number of tumor cells. In all 5 of these tumors, EdU label was also strongly detectable. In these 5 tumors, we consistently found that the set of BrdU+ cells included both EdU+ and EdU- negative cells, while all EdU+ cells were also BrdU+ (Figure 7D–F). The presence of BrdU+ cells that were EdU+ indicates that cells that were cycling 5 days after xRT gave rise to progeny that continued to divide. The presence of BrdU + cells that were EdU- cells indicates that some of the progeny of cells dividing 5 days after xRT either exited the cell cycle or proliferated more slowly.

To immunophenotype the BrdU+ tumors cells, we double labeled sections with antibodies to BrdU and either NeuN, PCNA or stem cell marker Sox2. Sox2 expressing cells have been associated with tumor recurrence in human medulloblastoma and have been shown to

behave as tumor stem cells, recapitulating recurrent medulloblastoma in Ptc mice treated with Ara-C [25]. We found in all 5 of the radiated, M-Smo;Bax^{floxed} mice with BrdU+ tumors, the BrdU labeled population included both NeuN+ and PCNA+ subpopulations (Figure 7G–L) indicating that cells that proliferate in the early period after xRT behaved like stem cells, giving rise to both differentiating and self-renewing progeny. Consistent with the neural stem cell phenotype, tumor cells that incorporated BrdU 5 days after xRT were predominantly Sox2+ 2 days later in all 5 mice examined (Figure 7 M–O). These results demonstrate that tumor stem cells that do not undergo apoptosis after xRT retain a proliferative capacity despite activation of p53. Considered against the more durable therapeutic response to cranial xRT in M-Smo tumors with intact p53 and Bax, the recurrence pattern after xRT in Bax-deficient medulloblastomas highlights the importance of inducing apoptosis in the stem cell population.

Discussion

Medulloblastoma is, on average, remarkably responsive to conventional treatment with xRT and chemotherapy. This susceptibility was discovered empirically, and the molecular basis for this susceptibility has not been defined. We have investigated the molecular mechanisms of treatment response in spontaneous medulloblastomas in transgenic, SmoM2 mice. We found that xRT produced a survival benefit in our model only when it activated a p53-dependent transcriptional response that induced apoptosis.

Medulloblastomas with conditional deletion of p53 were highly resistant to xRT. In these tumors, xRT did not induce either the pro-apoptotic or cell cycle regulatory arms of the p53-associated transcriptional response, demonstrated respectively by a lack of PUMA and p21 up-regulation after xRT. Consistent with the absence of these molecular events, tumors with p53 deletion did not undergo treatment-related apoptosis and resumed proliferation within 24 hours after treatment.

Medulloblastomas with Bax deletion were equally radiation resistant, despite having intact p53. The absence of apoptosis after xRT in these tumors made it possible to discern p53-dependent effects that would otherwise have been obscured by widespread cell death. Unlike p53-deficient tumors, radiated Bax-deficient tumors resolved into 2 distinct populations, as tumor cells either terminally differentiated or continued to proliferate. Terminally differentiated tumor cells expressed neuronal markers and formed Homer-Wright rosettes. Although rosettes are commonly observed in human medulloblastoma, the exaggerated abundance of rosettes in radiated M-SmoBax^{floxed} tumors recalls the histologic appearance of the highly malignant pediatric brain tumor known as Embryonal Tumor with Multilayered Rosettes (ETMR) [26]. Despite the increased differentiation of radiated, Bax-deleted medulloblastoma, these tumors progressed as rapidly as untreated tumors, due to the rapid growth of the proliferative component.

Paired BrdU/EdU experiments and immunophenotyping of BrdU+ tumor cells demonstrated the proliferative tumor cells that drove recurrence behaved as stem cells, giving rise to differentiating progeny and self-renewing proliferators. Prior investigations subjecting RCAS-induced, primary mouse medulloblastomas to 2Gy xRT showed that tumor stem cells

in the perivascular niche resumed proliferation within 72 hours of treatment [20]. We found that 10Gy xRT was sufficient to prevent early recurrence in M-Smo tumors, but only when the functions of both p53 and the intrinsic apoptotic pathway remained intact.

In mice with intact p53, Bax deletion allowed cells throughout the tumor to survive xRT. While p53 activation induced terminal differentiation in most cells of radiated, Bax-deficient tumors, perivascular stem cells did not undergo prolonged cell cycle arrest after treatment. The up-regulation of p21 in perivascular cells after xRT demonstrated that radiation provoked a p53-mediated response. In the absence of apoptosis, this p53-mediated transcriptional response was unable to prevent perivascular stem cells from repopulating the tumors. Thus perivascular stem cells were resistant to the p53-mediated cell cycle exit that led to differentiation outside of the perivascular regions. Taken together with the prior studies using lower dose xRT [20], our studies show that effective tumor treatment requires control of perivascular stem cells, through a dose of xRT that is sufficient to produce stem cell death through the intrinsic apoptotic pathway.

While we found that p53 function is required for response to xRT in our model, the relationship observed in medulloblastoma patients between p53 mutation and recurrence after therapy is complex [27–29]. Most medulloblastomas are radiosensitive and most medulloblastomas are p53 wild-type. Prior studies have shown in other tumors that p53 function is required for the susceptibility of cancer cells to DNA-damaging therapies [18, 19, 30–33]. In medulloblastoma patients, the effect of p53 mutation has depended on molecular subgroup. In the SHH subgroup of medulloblastoma, tumors with p53 mutation are significantly more likely to recur after treatment; in contrast, in the WNT subgroup, p53 mutation is not associated with recurrence [34]. All of the p53 mutations detected in these studies, however, were missense mutations, rather than deletions. Moreover, the mutations associated with the WNT and SHH subgroups were not equivalent. Specific mutant alleles may retain varying degrees of residual p53 function, and may also produce gains of function that affect prognosis [35]. Our model shows that complete loss of p53 function confers radiation resistance, consistent with the worse prognosis of Shh subgroup patients with mutant p53. The consequences of p53 missense mutations in human medulloblastoma must be interpreted in light of the subgroup context, the degree of residual p53 activity and potential gain of function.

We propose that loss of competence for apoptosis, downstream of p53, is a significant source of resistance to therapy. With variable impact and an overall frequency of about 5%, p53 mutations cannot account for the 20% rate of medulloblastoma recurrence. We found that even in tumors with intact p53, a single mutation in the apoptosis pathway is sufficient to cause radiation resistance. While Bax mutations have not been identified in medulloblastoma sequencing studies [36, 37] and Bax protein is consistently detected in patient-derived medulloblastoma samples [24], obstruction of apoptosis may be accomplished in cancer through diverse mechanisms, including up-regulation of anti-apoptotic Bcl-2 homologs and activation of Akt. Our previous finding that Bcl-2 expression correlates inversely with spontaneous apoptosis in patient-derived medulloblastoma samples, shows that Bax-dependent cell death is actively modulated by other proteins. Thus although Bax deletion does not directly model a genetic change seen in human medulloblastoma, the

principle demonstrated by Bax deletion, that apoptosis is required for treatment sensitivity, remains highly relevant. Moreover, this principle may be generalizable to other cancers, where inactivating frameshift mutations in Bax have been identified, including human colon cancer, gastric cancer and high grade glioma [38–41]. Our data indicate that any mutation or post-translational event that impairs the internal apoptotic pathway can confer treatment resistance.

Differentiation after DNA-damaging therapies has been observed in diverse cancers [42, 43]. We show that the combination of genotoxic stress, functional p53 and impaired apoptosis is sufficient to induce abundant differentiation, as xRT provoked neural differentiation in tumors with intact p53 and Bax deletion. We previously noted abundant intra-tumor differentiation in untreated, Bax-deficient medulloblastomas in the more slowly tumorigenic, ND2:SmoA1 mouse line; we interpreted terminal differentiation as an alternative fate choice for apoptosis-incompetent tumor cells with DNA damage that prevented continued proliferation [24]. In these untreated tumors, we ascribed DNA damage to replication stress. A similar histologic pattern was previously described in untreated medulloblastomas generated through simultaneous deletion of PTEN and overexpression of Shh [20]. In these tumors, PTEN loss caused activation of Akt, which may, like Bax deletion, effectively block apoptosis [44]. Taken together, these data show that the presence of differentiation in a tumor specimen, particularly after treatment, is not necessarily evidence of benign prognosis but rather may indicate defective apoptosis and increased risk of recurrence.

The similarity between radiated M-Smo;Bax^{floxed} medulloblastoma and ETMR suggests the possibility of a common mechanism. ETMR, like Bax-deleted medulloblastoma, is highly resistant to treatment. The pathogenesis of ETMR has been related to a fusion of the TTYH1 promoter with the C19MC microRNA cluster, ultimately leading to aberrant DNA methylation [45]. The mechanism of ETMR treatment resistance, however, is not known. Changes in DNA methylation, however, may plausibly alter the capacity for apoptosis, for example by changing the expression of key apoptosis-regulating proteins. Our data suggest that apoptosis resistance in the setting of genomic instability can produce differentiated pathology along with poor prognosis and should be suspected in malignant tumors such as ETMR that show abundant differentiation.

Supplementary Material

Refer to Web version on PubMed Central for supplementary material.

Acknowledgments

TRG is supported by grants from the National Institutes of Health (NIH; 1K08NS077978-01), the St. Baldrick's Foundation, and the American Institute for Cancer Research. This project is supported by a grant from the UNC University Cancer Research Fund. We thank the UNC Tissue Pathology Laboratory for expertise in immunohistochemistry.

References

1. Hanahan D, Weinberg RA. The Hallmarks of Cancer. Cell. 2000; 100(1):57–70. [PubMed: 10647931]

2. Hanahan D, Weinberg Robert A. Hallmarks of Cancer: The Next Generation. Cell. 2011; 144(5): 646–674. [PubMed: 21376230]

3. Brown JM, Attardi LD. The role of apoptosis in cancer development and treatment response. Nat Rev Cancer. 2005; 5(3):231–237. [PubMed: 15738985]

4. Okada H, Mak TW. Pathways of apoptotic and non-apoptotic death in tumour cells. Nature reviews. Cancer. 2004; 4(8):592–603. [PubMed: 15286739]

5. Patterson EFRF. Cerebellar medulloblastoma: treatment by irradiation of the whole central nervous system. Acta radiol. 1953; 39(4):323–336. [PubMed: 13057640]

6. Packer RJ, et al. Phase III Study of Craniospinal Radiation Therapy Followed by Adjuvant Chemotherapy for Newly Diagnosed Average-Risk Medulloblastoma. Journal of Clinical Oncology. 2006; 24(25):4202–4208. [PubMed: 16943538]

7. Cohen KJ, et al. Temozolomide in the treatment of high-grade gliomas in children: a report from the Children's Oncology Group. Neuro-oncology. 2011; 13(3):317–323. [PubMed: 21339192]

8. Ellison DW, et al. Medulloblastoma: clinicopathological correlates of SHH, WNT, and non-SHH/WNT molecular subgroups. Acta Neuropathologica. 2011; 121(3):381–396. [PubMed: 21267586]

9. Jones DT, et al. Dissecting the genomic complexity underlying medulloblastoma. Nature. 2012; 488(7409):100–105. [PubMed: 22832583]

10. Ellison DW, et al. Medulloblastoma: clinicopathological correlates of SHH, WNT, and non-SHH/WNT molecular subgroups. Acta Neuropathol. 2011; 121(3):381–396. [PubMed: 21267586]

11. Zurawel RH, et al. Evidence that haploinsufficiency of Ptch leads to medulloblastoma in mice. Genes Chromosomes Cancer. 2000; 28(1):77–81. [PubMed: 10738305]

12. Hallahan AR, et al. The SmoA1 mouse model reveals that notch signaling is critical for the growth and survival of sonic hedgehog-induced medulloblastomas. Cancer Research. 2004; 64(21):7794–7800. [PubMed: 15520185]

13. Hatton BA, et al. The Smo/Smo model: hedgehog-induced medulloblastoma with 90% incidence and leptomeningeal spread. Cancer Research. 2008; 68(6):1768–1776. [PubMed: 18339857]

14. Zurawel RH, et al. Analysis of PTCH/SMO/SHH pathway genes in medulloblastoma. Genes, Chromosomes and Cancer. 2000; 27(1):44–51. [PubMed: 10564585]

15. Mao J, et al. A Novel Somatic Mouse Model to Survey Tumorigenic Potential Applied to the Hedgehog Pathway. Cancer Research. 2006; 66(20):10171–10178. [PubMed: 17047082]

16. Schüller U, et al. Acquisition of Granule Neuron Precursor Identity Is a Critical Determinant of Progenitor Cell Competence to Form Shh-Induced Medulloblastoma. Cancer Cell. 2008; 14(2): 123–134. [PubMed: 18691547]

17. Schmitt CA, Rosenthal CT, Lowe SW. Genetic analysis of chemoresistance in primary murine lymphomas. Nature medicine. 2000; 6(9):1029–1035.

18. Lowe SW, et al. p53-dependent apoptosis modulates the cytotoxicity of anticancer agents. Cell. 1993; 74(6):957–967. [PubMed: 8402885]

19. Schmitt CA, Lowe SW. Apoptosis and chemoresistance in transgenic cancer models. Journal of molecular medicine. 2002; 80(3):137–146. [PubMed: 11894140]

20. Hambardzumyan D, et al. PI3K pathway regulates survival of cancer stem cells residing in the perivascular niche following radiation in medulloblastoma in vivo. Genes & Development. 2008; 22(4):436–448. [PubMed: 18281460]

21. Levine AJ, Oren M. The first 30 years of p53: growing ever more complex. Nature reviews. Cancer. 2009; 9(10):749–758.

22. Crowther AJ, et al. Tonic activation of Bax primes neural progenitors for rapid apoptosis through a mechanism preserved in medulloblastoma. The Journal of neuroscience : the official journal of the Society for Neuroscience. 2013; 33(46):18098–18108. [PubMed: 24227720]

23. Allen MA, et al. Global analysis of p53-regulated transcription identifies its direct targets and unexpected regulatory mechanisms. eLife. 2014; 3:e02200. [PubMed: 24867637]

24. Garcia I, et al. Bax deficiency prolongs cerebellar neurogenesis, accelerates medulloblastoma formation and paradoxically increases both malignancy and differentiation. Oncogene. 2012

25. Vanner RJ, et al. Quiescent sox2(+) cells drive hierarchical growth and relapse in sonic hedgehog subgroup medulloblastoma. Cancer Cell. 2014; 26(1):33–47. [PubMed: 24954133]
26. Korshunov A, et al. Embryonal tumor with abundant neuropil and true rosettes (ETANTR), ependymoblastoma, and medulloepithelioma share molecular similarity and comprise a single clinicopathological entity. Acta Neuropathologica. 2014; 128(2):279–289. [PubMed: 24337497]
27. Lindsey JC, et al. TP53 mutations in favorable-risk Wnt/Wingless-subtype medulloblastomas. Journal of clinical oncology : official journal of the American Society of Clinical Oncology. 2011; 29(12):e344–e346. author reply e347-8. [PubMed: 21357788]
28. Tabori U, et al. Universal poor survival in children with medulloblastoma harboring somatic TP53 mutations. Journal of clinical oncology : official journal of the American Society of Clinical Oncology. 2010; 28(8):1345–1350. [PubMed: 20142599]
29. Pfaff E, et al. TP53 mutation is frequently associated with CTNNB1 mutation or MYCN amplification and is compatible with long-term survival in medulloblastoma. Journal of clinical oncology : official journal of the American Society of Clinical Oncology. 2010; 28(35):5188–5196. [PubMed: 21060032]
30. Lowe SW, et al. p53 is required for radiation-induced apoptosis in mouse thymocytes. Nature. 1993; 362(6423):847–849. [PubMed: 8479522]
31. Schmitt CA, Lowe SW. Apoptosis and therapy. The Journal of pathology. 1999; 187(1):127–137. [PubMed: 10341713]
32. Schmitt CA, Lowe SW. Apoptosis is critical for drug response in vivo. Drug resistance updates : reviews and commentaries in antimicrobial and anticancer chemotherapy. 2001; 4(2):132–134. [PubMed: 11512522]
33. Johnstone RW, Ruefli AA, Lowe SW. Apoptosis: a link between cancer genetics and chemotherapy. Cell. 2002; 108(2):153–164. [PubMed: 11832206]
34. Zhukova N, et al. Subgroup-specific prognostic implications of TP53 mutation in medulloblastoma. Journal of clinical oncology : official journal of the American Society of Clinical Oncology. 2013; 31(23):2927–2935. [PubMed: 23835706]
35. Xu J, et al. Heterogeneity of Li-Fraumeni syndrome links to unequal gain-of-function effects of p53 mutations. Scientific reports. 2014; 4:4223. [PubMed: 24573247]
36. Pugh TJ, et al. Medulloblastoma exome sequencing uncovers subtype-specific somatic mutations. Nature. 2012; 488(7409):106–110. [PubMed: 22820256]
37. Rausch T, et al. Genome sequencing of pediatric medulloblastoma links catastrophic DNA rearrangements with TP53 mutations. Cell. 2012; 148(1–2):59–71. [PubMed: 22265402]
38. Yamamoto H, et al. Somatic frameshift mutations in DNA mismatch repair and proapoptosis genes in hereditary nonpolyposis colorectal cancer. Cancer Research. 1998; 58(5):997–1003. [PubMed: 9500462]
39. Rampino N, et al. Somatic frameshift mutations in the BAX gene in colon cancers of the microsatellite mutator phenotype. Science. 1997; 275(5302):967–969. [PubMed: 9020077]
40. Kim MS, et al. Rare somatic mutation of pro-apoptotic BAX and BAK genes in common human cancers. Tumori. 2012; 98(6):149e–151e.
41. Abdullah JM, et al. Molecular genetic analysis of BAX and cyclin D1 genes in patients with malignant glioma. Neurological research. 2007; 29(3):239–242. [PubMed: 17509221]
42. Brambilla E, et al. Cytotoxic chemotherapy induces cell differentiation in small-cell lung carcinoma. Journal of clinical oncology : official journal of the American Society of Clinical Oncology. 1991; 9(1):50–61. [PubMed: 1702146]
43. Sethi D, et al. Histopathologic changes following neoadjuvant chemotherapy in various malignancies. International journal of applied & basic medical research. 2012; 2(2):111–116. [PubMed: 23776823]
44. Wendel H-G, et al. Survival signalling by Akt and eIF4E in oncogenesis and cancer therapy. Nature. 2004; 428(6980):332–337. [PubMed: 15029198]
45. Kleinman CL, et al. Fusion of TTYH1 with the C19MC microRNA cluster drives expression of a brain-specific DNMT3B isoform in the embryonal brain tumor ETMR. Nature genetics. 2014; 46(1):39–44. [PubMed: 24316981]

46. Matei V, et al. Smaller inner ear sensory epithelia in Neurog1 null mice are related to earlier hair cell cycle exit. Developmental Dynamics. 2005; 234(3):633–650. [PubMed: 16145671]

47. Chow KH, et al. Epigenetic States of cells of origin and tumor evolution drive tumor-initiating cell phenotype and tumor heterogeneity. Cancer Research. 2014; 74(17):4864–4874. [PubMed: 25136069]

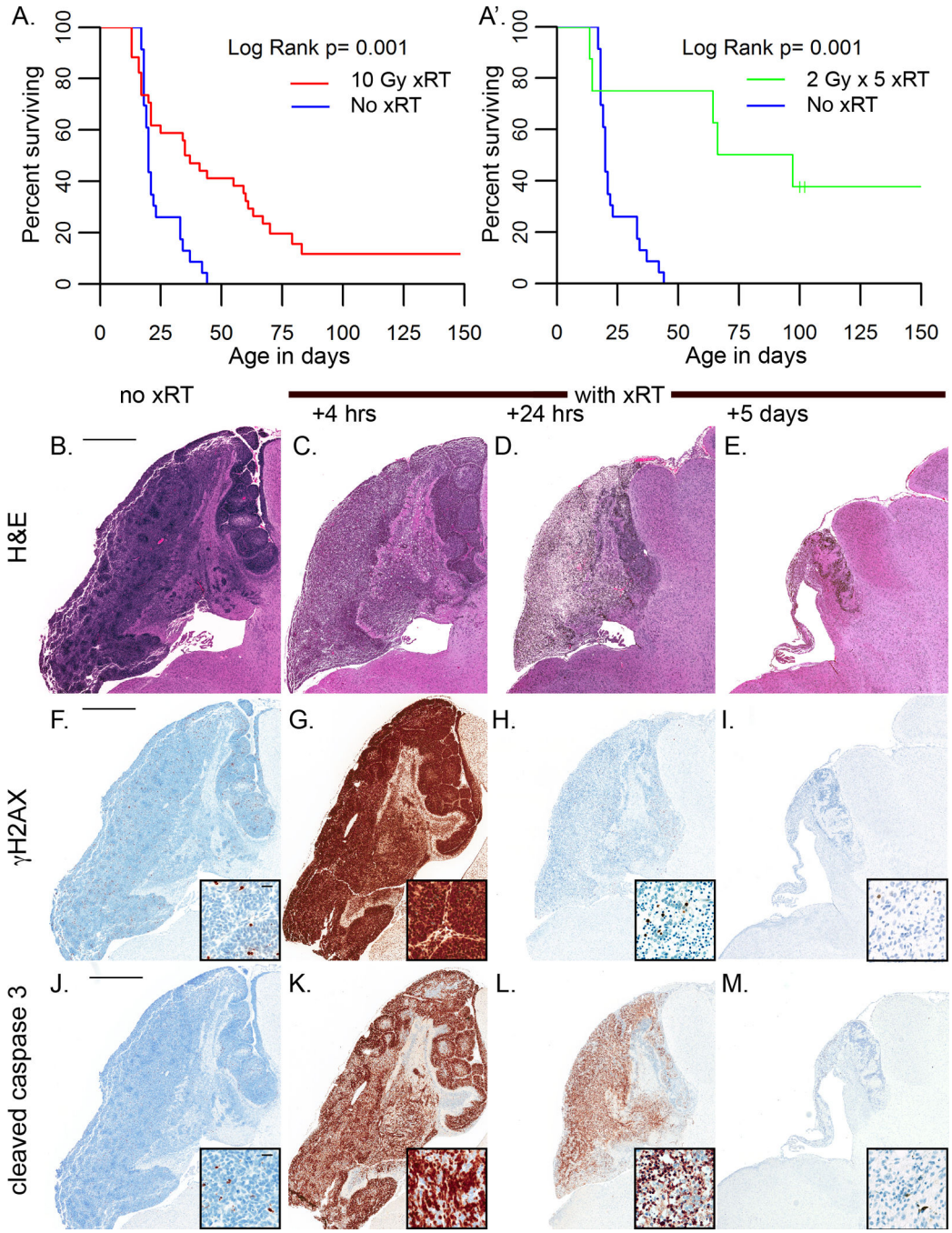

Figure 1. Medulloblastomas in M-Smo mice are radiation sensitive

A,A') Kaplan Meier curves demosntrated that xRT extends the survival of medulloblastoma-bearing mice. B–E) H&E stained sections of representative tumors harvested at the indicated interval after xRT. Tumors reduction is detectable 24 hours after xRT and is maximal by 5 days. F–I) IHC for γH2AX shows that cells with detectable DNA damage are rare in untreated tumors; xRT induces homogeneous γH2AX expression at 4 hours after xRT, that resolves by 24 hours. J–M) IHC for cC3 shows that apoptotic cells are rare in untreated tumors. Radiation induces widespread apoptosis by 4 hours after treatment. Apoptosis

continues through 24 hours after xRT. By 5 days, apoptotic cells are rare within the residual tissue that persists after xRT. Scale bars are 1mm in low power images and 20 μm in insets.

A.

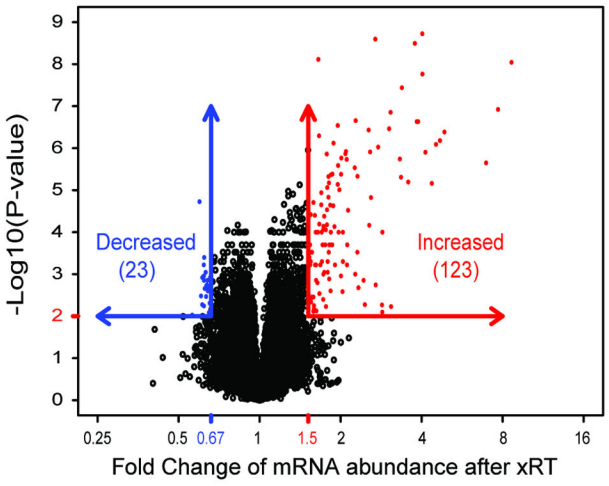

C.

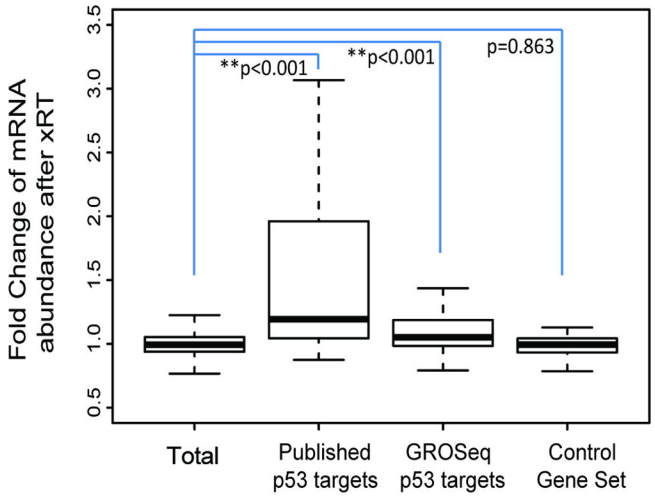

B.

Description of enriched gene sets	FDR BH	Reference
p53 responsive genes in both fetal liver and neuroepithelium using MDM4 knockout model.	1.65E-30	Martoriati, Alain, *et al.*
Genes up-regulated in neural stem cells (NSC) at 60 h after cre-lox knockout of TLX (NR2E1).	1.15E-25	Zhang, Chun-Li, *et al.*
Genes up-regulated in MEF cells lacking p53 and BRCA1 by expression of p53.	9.70E-21	Ongusaha, Pat P., *et al.*
Genes up-regulated in p53 normal cells (breast cancer) exposed to doxorubicin in the presence of medium concentrate from p53 mutated cells.	4.07E-19	Graessmann, M., *et al.*
Genes up-regulated in p53 normal cells (breast cancer) undergoing apoptosis in response to doxorubicin.	1.36E-17	Graessmann, M., *et al.*

D.

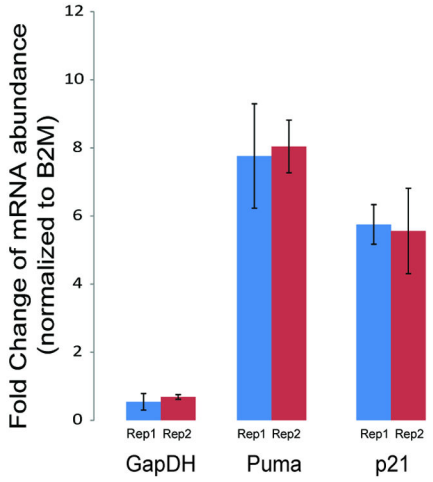

Figure 2. Increased expression of p53 targets mediating apoptosis and cell cycle arrest after xRT

A) Quantification of mRNA abundance after xRT based on expression microarray data. B) The five most enriched gene sets from the genes with increased expression using GSEA analysis (see supplementary table 1). C) Comparison of mRNA abundance change after xRT among indicated gene sets (see supplementary table 2). P-values are estimated by permutation. D) Fold change in the abundance of mRNA for Puma, p21 and GAPDH when radiated and untreated M-Smo tumors are compared (n=3 for each group). Abundance of mRNA was measured by quantitative RT-PCR and normalized to the abundance of β2 Microglobulin (B2M) mRNA. Puma and p21 are induced by xRT, while GAPDH abundance is not significantly altered.

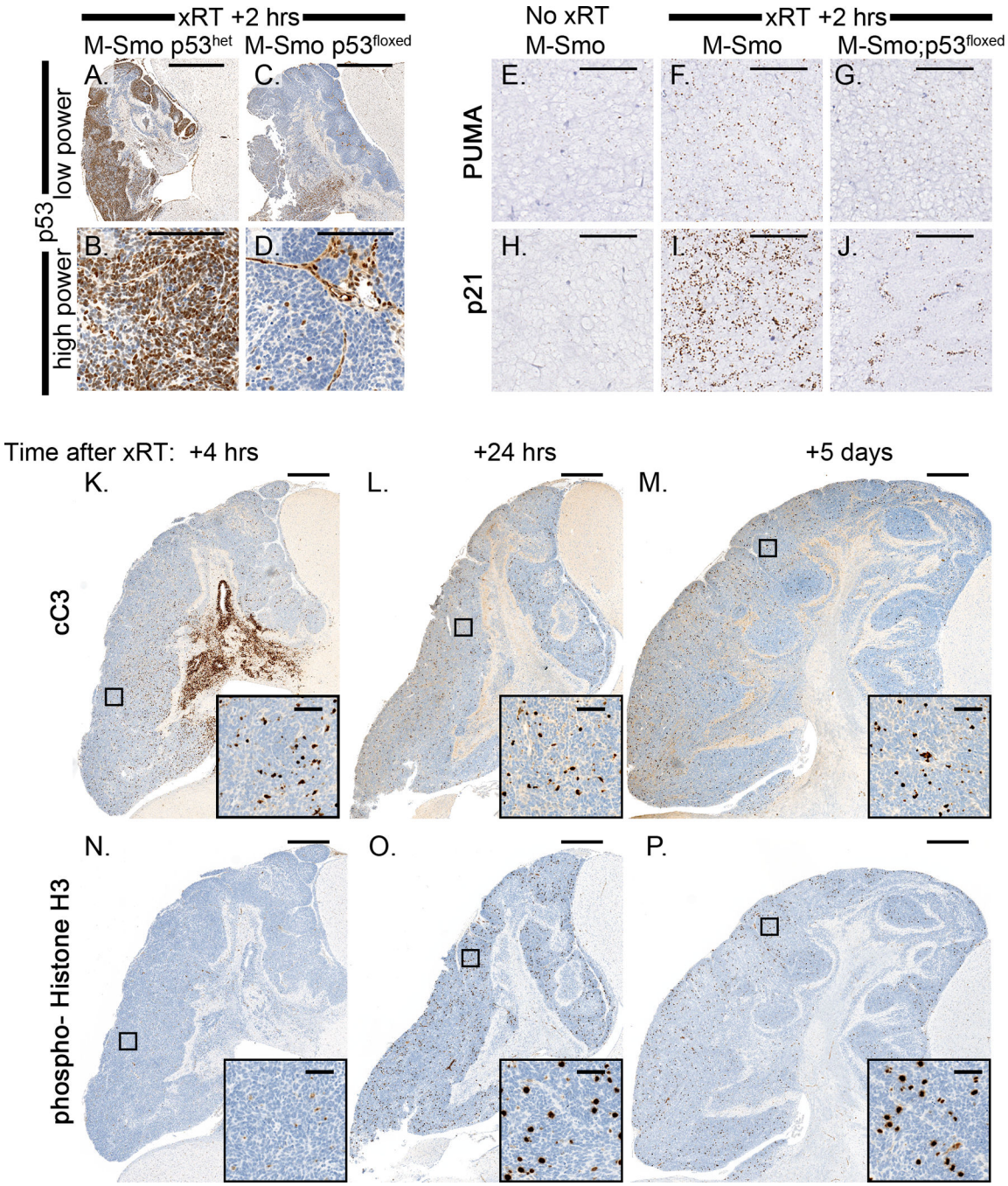

Figure 3. Conditional deletion of p53 abrogates the treatment response to xRT

A,B) IHC for p53 demonstrates accumulation of p53 protein 2 hours after xRT in M-Smo tumors with intact p53. C,D) In M-Smo;p53^{floxed} tumors, p53 is absent in tumor cells but detectable in adjacent stroma and in endothelial cells within the tumors. E–J) *In situ* hybridization demonstrates mRNA for Puma and p21 as indicated. Both Puma and p21 mRNAs are induced by xRT in M-Smo tumors. Post-xRT expression of Puma and p21 is reduced in tumors with conditional deletion of p53. K–M) Cleavage of caspase 3 is not induced in M-Smo;p53^{floxed} tumors by xRT at either 4 hours, 24 hours or 5 days after

treatment. N–P) IHC for PH3 demonstrates mitotic figures. M-Smo;$p53^{floxed}$ tumors demonstrate absence of mitosis 4 hours after xRT, but demonstrate frequent mitoses 24 hours and 5 days after treatment. Scale bars: 1mm (A,C and K–P), 100 μm (B,D and E–J), and 50 μm (insets).

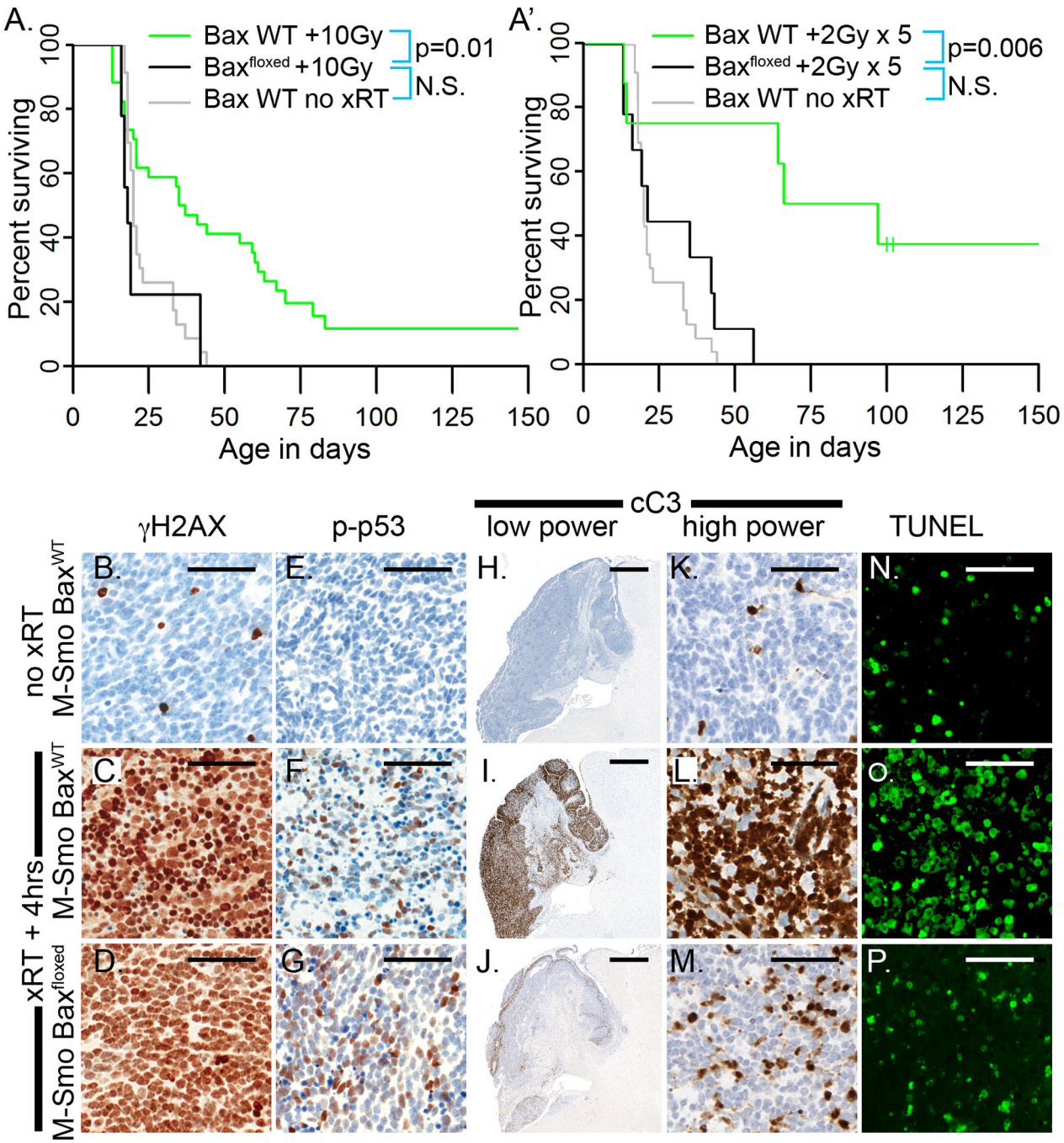

Figure 4. Medulloblastomas with Bax deletion are resistant to xRT despite activation of p53

A,A') Kaplan Meier curves compare the survival of radiated M-Smo;Bax^{floxed} mice to radiated and untreated M-Smo mice. Log Rank analysis shows that the difference in the survival of radiated mice with intact or deleted alleles of Bax is statistically significant. B–G) xRT induces γH2AX (B–D) and phosphorylation of p53 (E–G) in medulloblastomas of both M-Smo and M-Smo;Bax^{floxed} mice. H–M) IHC for cC3 demonstrates that apoptosis is strongly induced by xRT in M-Smo tumors, but greatly reduced in M-Smo;Bax^{floxed} tumors.

N–P) TUNEL staining similarly demonstrates that cell death after xRT is greatly reduced in tumors with Bax deletion. Scale bars: 50 μm (B–-G and K–P), 100 μm (H–J).

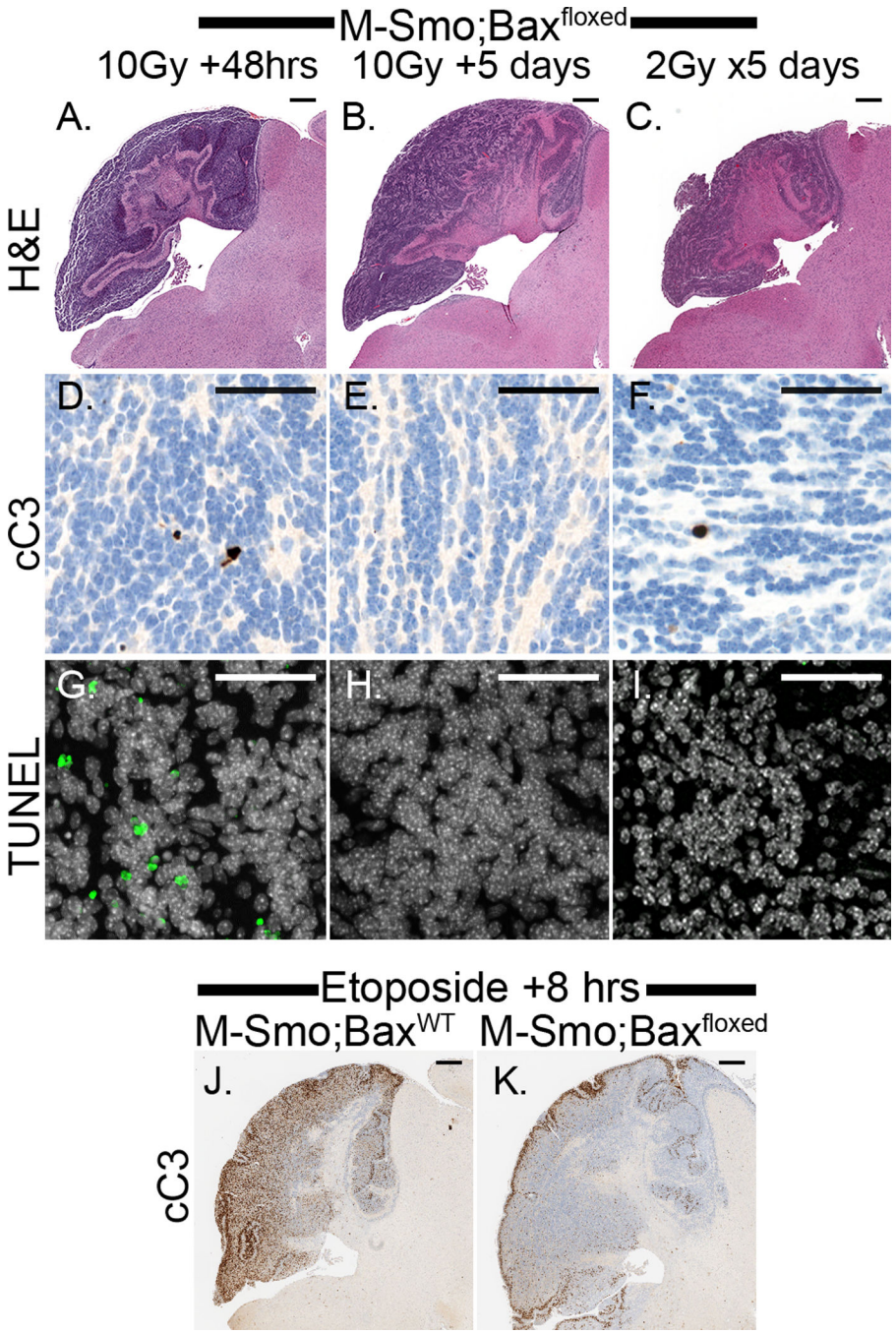

Figure 5. Absence of cell death in medulloblastoma with Bax deletion after xRT or chemotherapy

A–C) H&E stained sections of representative, radiated M-Smo;Bax^{floxed} tumors at (A) 48 hours after 10 Gy, (B) 5 days after 10 Gy, and (C) after 5 daily doses of 2Gy consistently do not demonstrate tumor regression typical of medulloblastoma with intact Bax. D–I) cC3 and TUNEL staining do not demonstrate widespread apoptosis at the indicated interval after treatment. J,K) IHC for cC3 shows apoptosis in an M-Smo tumor 8 hours after etoposide treatment. Markedly less apoptosis is induced by etoposide in a representative M-Smo;Bax^{floxed} tumor. Scale bars: 500 μm (A–C and J,K), 50 μm (D–I).

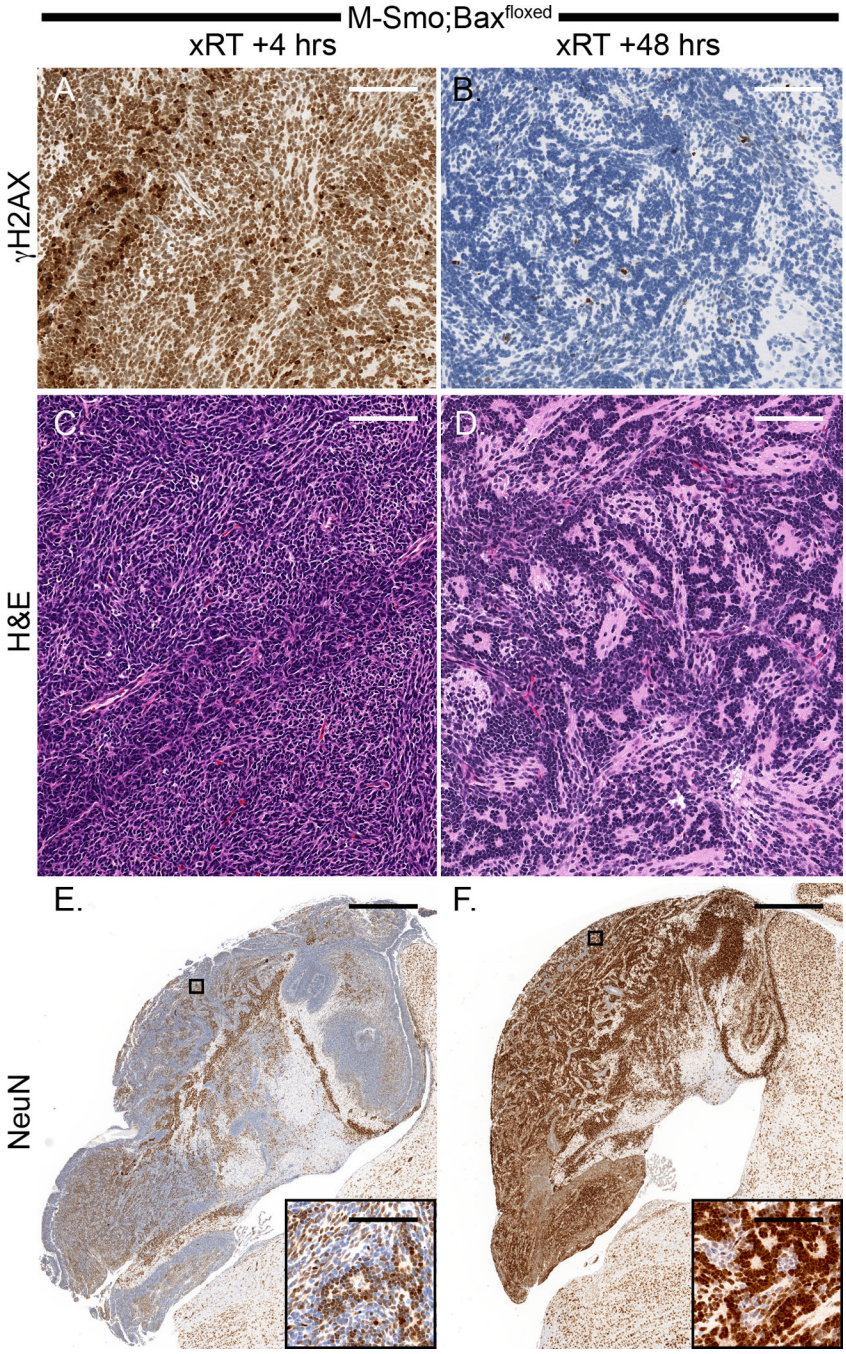

Figure 6. Radiation induced changes in Bax-deleted medulloblastomas: DNA repair and neuronal differentiation

A,B) γH2AX, strongly detectable 4 hours after xRT resolved by 48 hours, consistent with effective DNA repair. C,D) Between 4 and 48 hours after xRT, M-Smo;Bax^{floxed} medulloblastomas developed a differentiated histology, marked by the elaboration of eosinophilic neuropil and the formation of Homer Wright rosettes. E,F) IHC for NeuN demonstrates the dramatic increase in NeuN expression that was consistently seen 48 hours after radiation of Bax-deleted tumors. Scale bars: 100 μm (A–D and insets), 1 mm (E,F).

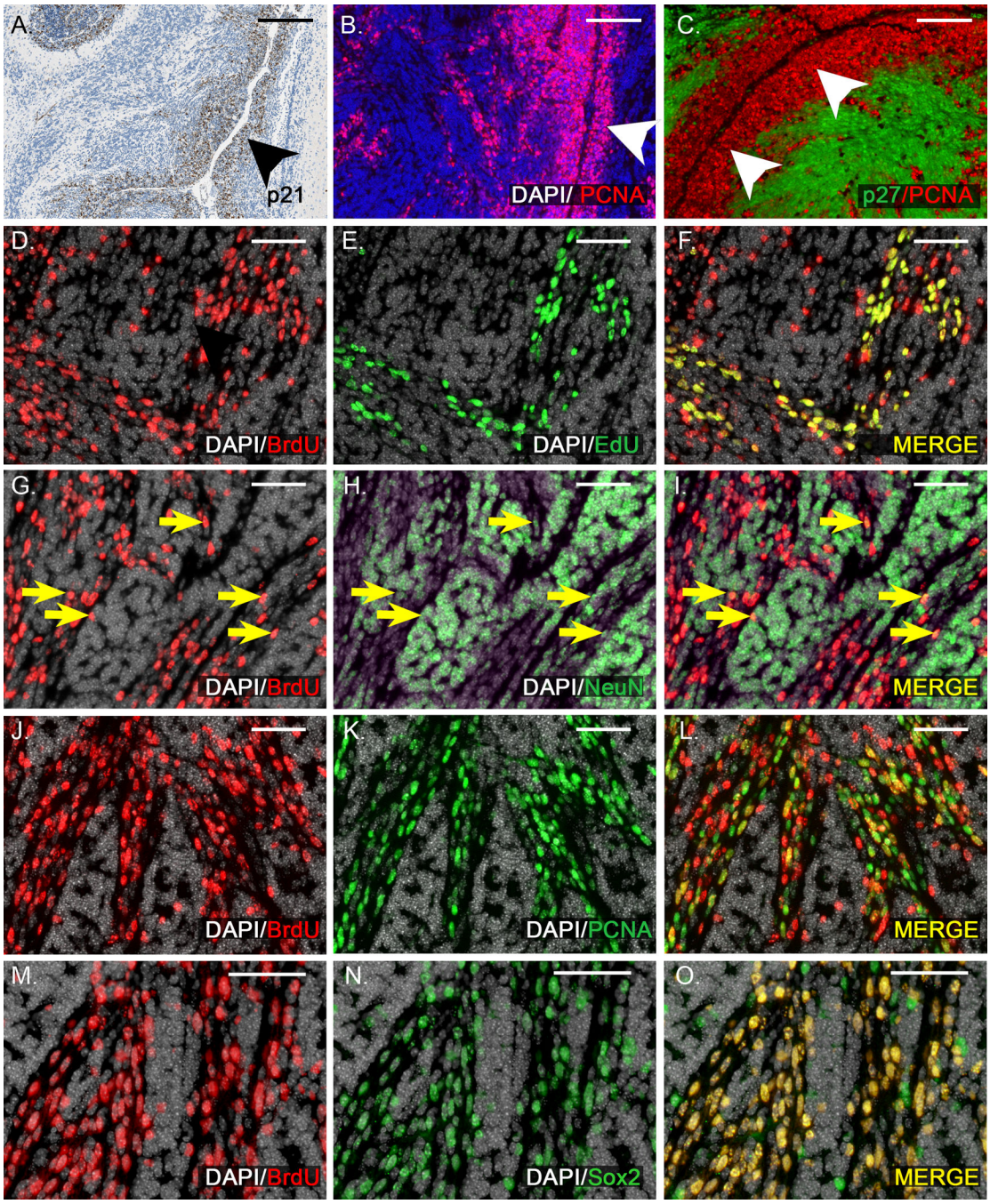

Figure 7. In apoptosis-deficient tumors, xRT fails to prevent the growth of perivascular stem cells that drive recurrence

A) IHC demonstrates p21 up-regulation specifically in cells of the perivascular region (arrowhead) 4 hours after xRT. B) 48 hours after xRT, cells of the perivascular region (arrowhead) express proliferation marker PCNA. C) Double labeling with antibodies to PCNA and differentiation marker p27 demonstrates proliferation in the perivascular region (arrowheads) and differentiation further from the vessels. D–F) BrdU injected 5 days after xRT labels a subpopulation of tumor cells in a representative M-Smo;Bax^{floxed} tumor. EdU injection 2 hours prior to harvest labels an overlapping subpopulation. All EdU+ cells were

BrdU+, indicating that cells proliferating 7 days after xRT descend from cells proliferating 2 days earlier. Some BrdU+ cells were EdU- consistent with a portion of BrdU+ cells having left the cell cycle. G–I) In the same tumor, a portion of BrdU+ cells express NeuN (yellow arrows), consistent with neuronal differentiation. J–L) In the same tumor, numerous BrdU+ cells are PCNA+, indicating continued proliferation. M–O) BrdU+ cells were predominantly Sox2+, consistent with a stem cell phenotype. Scale bars: 100 μm (A–C), 50 μm (D–O).